Proceedings of the SPIE Conference on Automatic Target Recognition XII **4726**. April, 2002.

GLINT INDUCED FALSE ALARM REDUCTION IN SIGNATURE ADAPTIVE TARGET DETECTION

Frank Crosby
Naval Surface Warfare Center, Coastal Systems Station, Panama City, FL 32407

ABSTRACT

The signal adaptive target detection algorithm developed by Crosby and Riley uses target geometry to discern anomalies in local backgrounds. Detection is not restricted based on specific target signatures. The robustness of the algorithm is limited by an increased false alarm potential. The base algorithm is extended to eliminate one common source of false alarms in a littoral environment. This common source is glint reflected on the surface of water. The spectral and spatial transience of glint prevent straightforward characterization and complicate exclusion. However, the statistical basis of the detection algorithm and its inherent computations allow for glint discernment and the removal of its influence.

Keywords: ATR, CFAR**,** multispectral detection, Glint, False Alarm Reduction**.**

1. INTRODUCTION

The exploitation of spectral differences using multispectral processing is complicated by highly variable target and background signatures. To address this problem, a signature adaptive algorithm was designed. The basis of this algorithm is a local analysis to determine spectral anomalies with an estimated shape[1]. Its detection threshold depends only on the number of spectral bands and the number of pixels in samples. Since the threshold only depends on these two numbers, it is said to detect targets at a constant false alarm rate. Furthermore, it adapts to a changing environment and target signatures by estimating conditions based on the observed data.

As with most signature adaptive algorithms, it owes much of its success to the limited assumptions placed on the data. A limited number of assumptions allow it to be successful in many different situations. However, as a result it can be more susceptible to false alarms than other algorithms that depend on a priori target information.

One prolific source of false alarms that arises in passive multispectral sensing in the littoral environment is the reflection of sunlight off of the surface of water. Achieving reliable detection performance requires that false alarms produced by this glint be mitigated. Glint often appears as localized anomalies that have the same shape as targets of interest. The similarity in shape prevents discrimination based on morphology. However, the spectral signature of glint is significantly different from most targets. Although the spectral signature of glint is its key feature, it is not invariable. The variability of glint prevents a straightforward categorization of glint as being a bright response in each of the multispectral bands. Using the spectral signature of glint to prevent false alarms requires that both spatial and spectral variability be accommodated.

The algorithm modification presented in this paper reduces false alarms due to glint while retaining the adaptability of the original target detection method. The following section describes the detection model and highlights the development of the algorithm from the statistical assumptions. The third section shows the glint model and how the existing detection calculations can be used to eliminate false alarms due to glint. That is followed by a demonstration of the algorithm's performance on actual data. The results show the algorithm modification to be very effective.

2. DETECTION MODEL

Previous studies have found that multispectral optical images can be locally modeled as independent Gaussian processes. Performing local analysis reduces the possibility of encountering samples with several spectral distributions. The goal is to

analyze an area that contains either a single spectral category or a single category and a target. The local area surrounding the possible target area is modeled with a normal distribution. The target is also assumed to have a normal distribution and share a common covariance matrix with the surrounding area.

The goal is to determine if an area contains, as a subset, an object of interest. The null hypothesis is that there is no object present. If there is no object present, then the mean of the surrounding area will be similar to the mean of the possible target area. The alternative hypothesis is that there is an object present. If there is an object, then the two means will be different.

In statistical terms, the distributions are assumed to be normal with means $\mu_{\mathbf{B}}$ and $\mu_{\mathbf{T}}$ and common covariance Σ, denoted $N(\mu_{\mathbf{B}}, \Sigma)$ and $N(\mu_{\mathbf{T}}, \Sigma)$. The hypotheses are:

$$H_0 : \mu_{\mathbf{B}} = \mu_{\mathbf{T}}$$
$$H_1 : \mu_{\mathbf{B}} \neq \mu_{\mathbf{T}}$$

In p-band multispectral images, each pixel is a p-dimensional sample, $\mathbf{x}_i = [x_1 \cdots x_p]^{\mathrm{T}}$. A local sample of the image of size *N* is given by $\mathbf{X} = [\mathbf{x}_1 \cdots \mathbf{x}_N]$. This sample is divided into two disjoint sets, background pixels, $\mathbf{B} = [\mathbf{b}_0, \ldots, \mathbf{b}_{N_{\mathbf{B}}}]$, and possible target pixels, $\mathbf{T} = [\mathbf{t}_0, \ldots, \mathbf{t}_{N_{\mathbf{T}}}]$. The test is based on pixels that are either background or possible target pixels, mixed pixels are ignored. Therefore, $N_{\mathbf{B}} + N_{\mathbf{T}} = N$. The mean of the background is given by $\sum_{N_{\mathbf{B}}} \mathbf{b} \Big/ N_{\mathbf{B}} = \mu_{\mathbf{B}}$. Let $\bar{\mathbf{b}}$ be a vector of the same length as **B** each element of which is identical and equal to $\mu_{\mathbf{B}}$.The mean of the target pixels are given by $\sum_{N_{\mathbf{T}}} \mathbf{t} \Big/ N_{\mathbf{T}} = \mu_{\mathbf{T}}$. Let $\bar{\mathbf{t}}$ be a vector of the same length as **T** each element of which is identical and equal to $\mu_{\mathbf{T}}$.

The likelihood function for a background and target sample is given by

$$L(\mu_{\mathbf{B}}, \mu_{\mathbf{T}}, \Sigma) = \left(\frac{1}{(2\pi)^p \left|\Sigma\right|^p} \right)^{N_{\mathbf{B}}/2} \exp\left(\frac{-1}{2} \sum_{i=0}^{N} (\mathbf{b}_i - \mu_{\mathbf{B}})^{\mathrm{T}} \Sigma^{-1} (\mathbf{b}_i - \mu_{\mathbf{B}}) \right)$$
$$\cdot \left(\frac{1}{(2\pi)^p \left|\Sigma\right|^p} \right)^{N_{\mathbf{T}}/2} \exp\left(\frac{-1}{2} \sum_{j=0}^{M} (\mathbf{t}_j - \mu_{\mathbf{T}})^{\mathrm{T}} \Sigma^{-1} (\mathbf{t}_j - \mu_{\mathbf{T}}) \right)$$
$$= \left((2\pi)^p\right)^{-(N)/2} \left(\left|\Sigma\right|^{-1} \right)^{N/2} \exp\left(\frac{-1}{2} \left(\sum_{i=1}^{N_{\mathbf{B}}} (\mathbf{b}_i - \mu_{\mathbf{B}})^{\mathrm{T}} \Sigma^{-1} (\mathbf{b}_i - \mu_{\mathbf{B}}) + \sum_{i=1}^{N_{\mathbf{T}}} (\mathbf{t}_i - \mu_{\mathbf{T}})^{\mathrm{T}} \Sigma^{-1} (\mathbf{t}_i - \mu_{\mathbf{T}}) \right) \right),$$

which is also the joint probability distribution function.

If there is no target present, then $\mu_{\mathbf{B}} - \mu_{\mathbf{T}} = 0$. The common mean is denoted $\mu = \mu_{\mathbf{B}} = \mu_{\mathbf{T}}$. The maximum likelihood estimate of the mean is given by

$$\hat{\mu} = \frac{\sum_{i=1}^{N_{\mathbf{B}}} \mathbf{b}_i + \sum_{i=1}^{N_{\mathbf{T}}} \mathbf{t}_i}{N_{\mathbf{B}} + N_{\mathbf{T}}}.$$

The maximum likelihood estimate of the covariance is given by

$$\hat{\Sigma} = \frac{1}{N}\left[\sum_{i=1}^{N_{\mathbf{B}}}(\mathbf{b}_i - \mu_{\mathbf{B}})^{\mathrm{T}}(\mathbf{b}_i - \mu_{\mathbf{B}}) + \sum_{i=1}^{N_{\mathbf{T}}}(\mathbf{t}_i - \mu_{\mathbf{T}})^{\mathrm{T}}(\mathbf{t}_i - \mu_{\mathbf{T}})\right]$$
$$= \frac{1}{N}\left[(\mathbf{B} - \bar{\mathbf{b}})^{\mathrm{T}}(\mathbf{B} - \bar{\mathbf{b}}) + (\mathbf{T} - \bar{\mathbf{t}})^{\mathrm{T}}(\mathbf{T} - \bar{\mathbf{t}})\right].$$

If a target is present, then

$\hat{\mu}_{\mathbf{B}} = \frac{1}{N_{\mathbf{B}}}\sum_{i=1}^{N}\mathbf{b}_i$ and $\hat{\mu}_{\mathbf{T}} = \frac{1}{N_{\mathbf{T}}}\sum_{i=1}^{M}\mathbf{t}_i$ are distinct and $\hat{\Sigma}$ remains unchanged.

Establishing a test with a constant false alarm rate is based on the probability of rejecting H_0 when H_0 is true. The set of points in the parameter space that corresponds to a rejection of the null hypothesis is called the critical region. The critical region depends on both the joint probability density function and the desired false alarm rate. Let ω be the set of points in the parameter space that correspond to H_0 and Ω be the set of all points in the parameter space. For our example, $\omega = \{(\mu_{\mathbf{B}}, \mu_{\mathbf{T}}) : \mu_{\mathbf{B}} = \mu_{\mathbf{T}}, -\infty < \mu_{\mathbf{B}}, \mu_{\mathbf{T}} < \infty\}$ and $\Omega = \{(\mu_{\mathbf{B}}, \mu_{\mathbf{T}}) : -\infty < \mu_{\mathbf{B}}, \mu_{\mathbf{T}} < \infty\}$.

By utilizing the likelihood function we can judge if a particular sample of the background and target does not support H_0. Let the sample be given and let $L(\hat{\omega})$ be the likelihood function maximized with respect to parameters in ω, and let $L(\hat{\Omega})$ be the likelihood function maximized with respect to parameters in Ω. One would expect that if the sample does not support H_0, then $L(\hat{\omega})$ would be much smaller than $L(\hat{\Omega})$. This was formally proven by Neyman-Pearson in their generalized maximum likelihood ratio criterion. The criterion states that the critical region for a test of H_0 against H_1 is defined by the set of points in the sample space for which $\frac{L(\hat{\omega})}{L(\hat{\Omega})} \le k$, where k is selected so that $P(\frac{L(\hat{\omega})}{L(\hat{\Omega})} < k \mid H_0 \text{ true}) \le \alpha$, where α is the desired false alarm rate.

The inequality $\frac{L(\varpi)}{L(\Omega)} \le k$ leads to the test

$$F(\mathbf{X}) = \frac{N_{\mathbf{B}}N_{\mathbf{T}}}{N}(\mu_{\mathbf{B}} - \mu_{\mathbf{T}})^{\mathrm{T}}\mathbf{S}^{-1}(\mu_{\mathbf{B}} - \mu_{\mathbf{T}})$$

where $\mathbf{S} = \frac{1}{N-2}\left[(\mathbf{B} - \bar{\mathbf{b}})^{\mathrm{T}}(\mathbf{B} - \bar{\mathbf{b}}) + (\mathbf{T} - \bar{\mathbf{t}})^{\mathrm{T}}(\mathbf{T} - \bar{\mathbf{t}})\right]$.

The distribution of $F(\mathbf{X})$ is a central F-distribution in the case that the null hypothesis is true.

3. GLINT MODEL

Multispectral detection that is based on differences in the visual wavelengths are of optimal use during times when the sun is at its highest. During these times, when the zenithal angle is small, shadows are reduced and the spectral response differences are dominated by reflectance characteristics. In addition, underwater targets are the most visible since the amount of light penetrating the sea surface drops off sharply with increased sun zenithal angle. The combination of a downward sensing camera and a small sun zenithal angle mean that glint can be a common occurrence.

The dominate feature of glint is that areas of glint are significantly brighter that the local background. Although the strength of multispectral processing is its ability to exploit spectral energy differences between targets and their surroundings, glint easily qualifies as a local anomaly. Profiles of glint show how much brighter it is than the surroundings. Figure 1 shows a enlarged view of an element of glint. Figure 2 shows a histogram of the pixel values fit with a Gaussian curve. The Gaussian distribution gives a good approximation given that the number of samples is very limited. A Gaussian distribution is one of the assumptions in the detection model. Thus, glint is similar to targets in this respect.

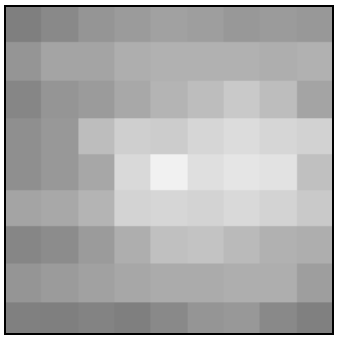

Figure 1: Enlarged element of glint.

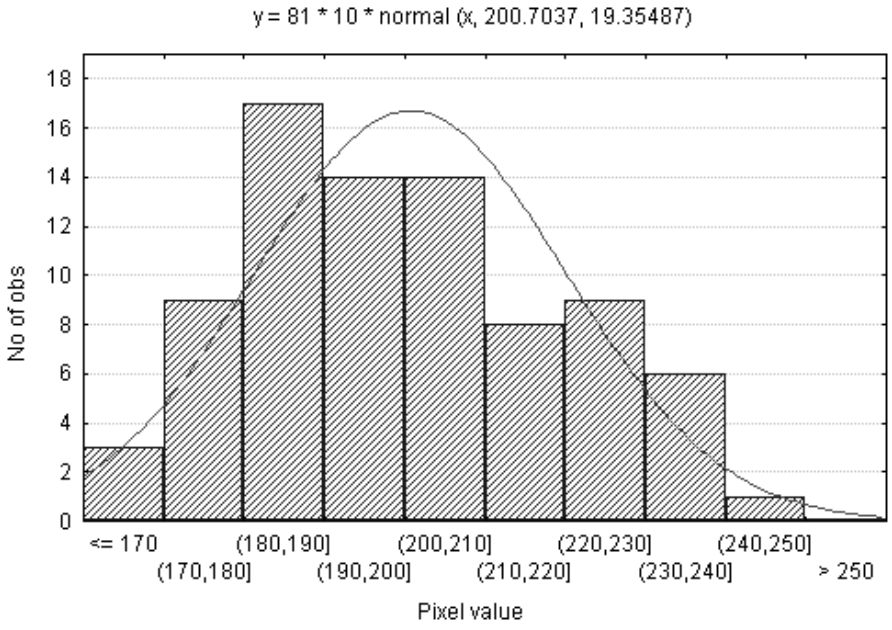

Figure 2: Glint histogram.

Glint can also appear in a variety of shapes. These shapes often exhibit the same kind of symmetry that targets of interest are assumed to possess. Figure 3 shows a three-dimensional representation of the element of glint with pixel intensity as the z-axis. The change in pixel values is fairly uniform about the center, which indicates a circular phenomenon similar to many targets.

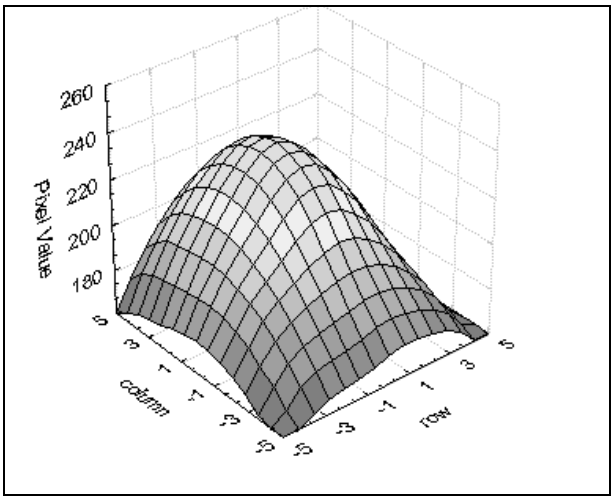

Figure 3: Three-dimensional representation of glint.

There are two primary difficulties that must be addressed in the characterization of glint. One is that the exact image intensity is highly variable. Figure 4 displays dual band scatterplot of some pixel values associated with glint. Very few of the pixels show eight-bit saturation in both bands. Most of the pixels show saturation in one of the bands. However, there are many that do not show saturation in either band.

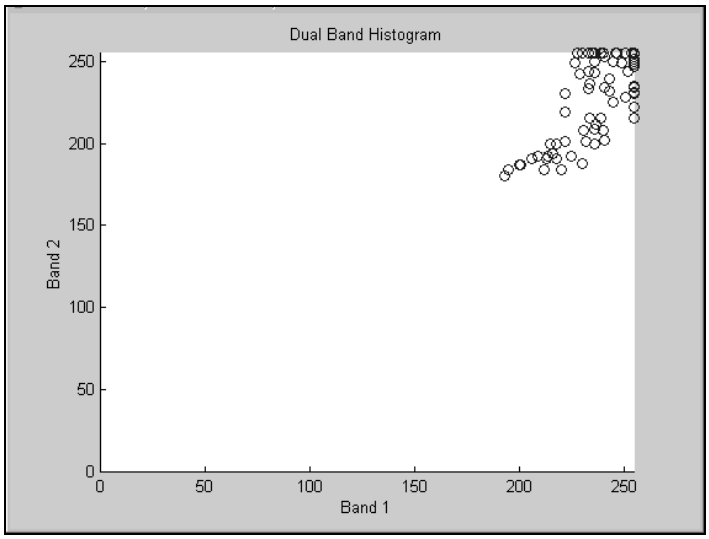

Figure 4. Dual Band scatterplot of glint.

Another difficultly is that glint is highly transient. Glint is a factor of two rapidly changing perspectives. The sensor platform and the water surface can cause a spot of glint to disappear rapidly. In a framing filter wheel camera at standard video rates, glint can easily change in successive frames and disappear between the first and last band. Figure 5 shows glint in successive frames of a framing filter wheel camera. The change in the glint is evident.

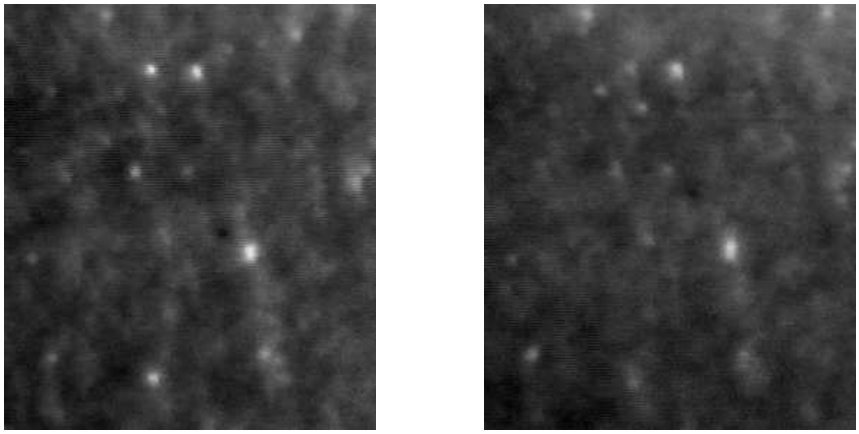

Figure 5: Successive frames showing glint.

Cameras that capture all bands simultaneously are not as susceptible to the transitory nature of glint. However, even slight registration offsets, perspective differences, and filter transmission variances can result in a pixel that achieves maximum brightness in a single band and not in the other bands. An example is shown in Figure 6.

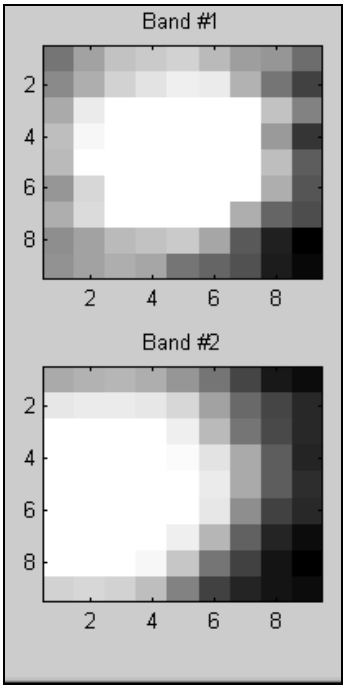

Figure 6: Simultaneously captured close-ups of glint.

Targets often appear lighter than their local background in some of the bands. Our studies have shown that rarely do targets appear brighter in all bands. Figure 7 shows a scene with two targets highlighted. The targets are lighter than the background. Figure 8 shows the same targets in a different band where the targets are darker than their surroundings.

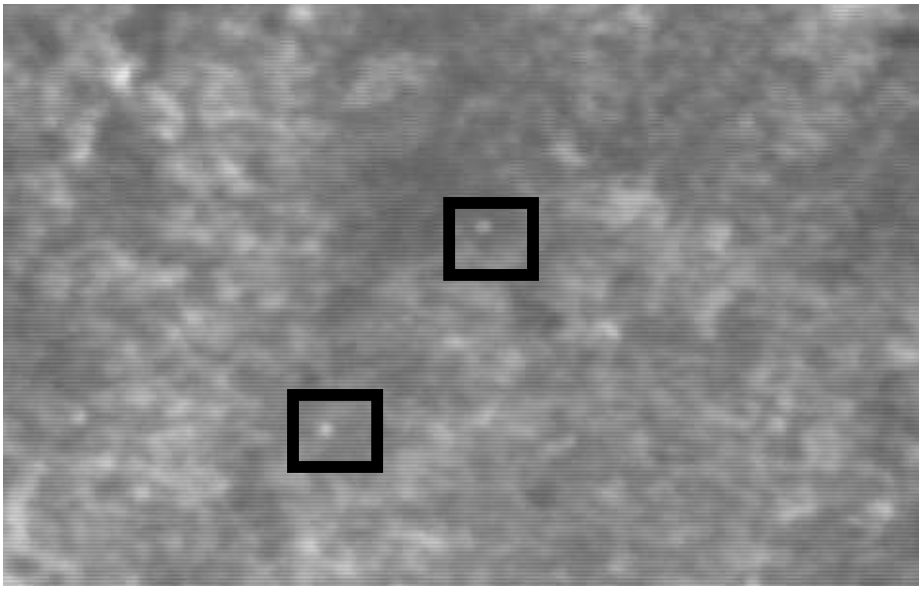

Figure 7: Target in a grass field at a lower wavelength.

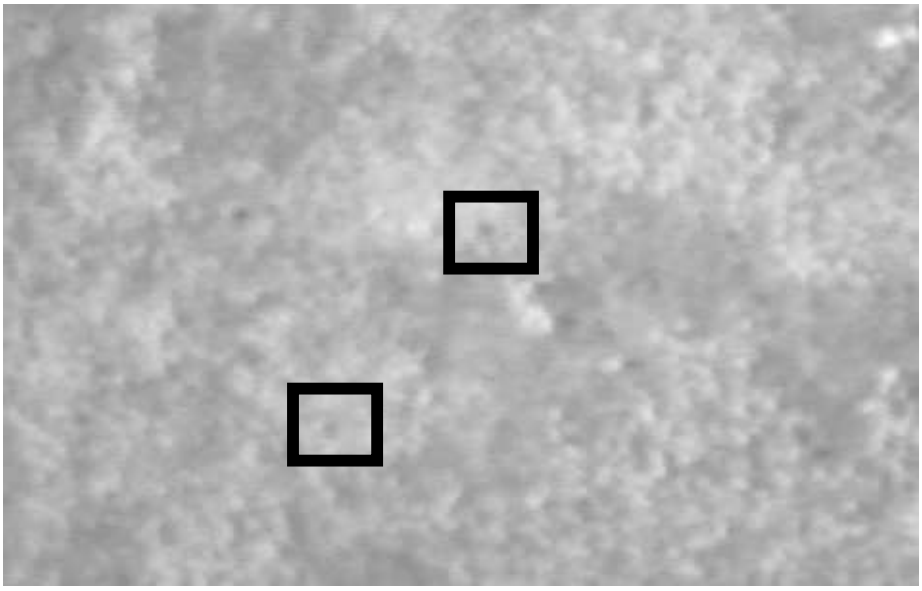

Figure 8: Target in a grass field at a higher wavelength.

Glint can be generally classified as an anomaly that has a very high reflectance in at least one channel. Since the detection of brightness is complicated by the spectral variability of glint, the absence of darkness was chosen as the test of glint.
The assumptions placed on the data in the development of the detection algorithm are on the general distribution type of the backgrounds and targets. There are no restrictions placed on the mean intensity in any of bands. Furthermore, the relationship between the background mean and the target mean is allowed to fluctuate.

The detection criterion is based on finding $\mu_{\mathbf{B}} - \mu_{\mathbf{T}}$. By assumption, the variance of the background is the same as the target area. The standard deviation in band *k* is given by

$$\begin{aligned}\sigma^2 &= \frac{1}{N}\left[([\mathbf{B}]_k - [\mu_{\mathbf{B}}]_k)^{\mathrm{T}}([\mathbf{B}]_k - [\mu_{\mathbf{B}}]_k) + ([\mathbf{T}]_k - [\mu_{\mathbf{T}}])^{\mathrm{T}}([\mathbf{T}]_k - [\mu_{\mathbf{T}}])\right] \\ &= \left[\frac{1}{N-2}\left[(\mathbf{B}-\bar{\mathbf{b}})^{\mathrm{T}}(\mathbf{B}-\bar{\mathbf{b}}) + (\mathbf{T}-\bar{\mathbf{t}})^{\mathrm{T}}(\mathbf{T}-\bar{\mathbf{t}})\right]\right]_{kk} \\ &= \mathbf{S}_{kk}.\end{aligned}$$

The background is assumed to be normally distributed. As such, the standard deviation provides a useful guide for many data sets:

- About 68% of data lie within one standard deviation of the mean.
- About 95% of data lie within two standard deviations of the mean.
- And almost all data lie within three standard deviations of the mean

Choosing a threshold of 1.5 standard deviations selects points with a significant dark component. If $\frac{(\mu_{\mathbf{B}} - \mu_{\mathbf{T}})}{\sqrt{\mathbf{S}_k}} > 1.5$ for some $k \in \{1, \ldots, p\}$, then $\mathbf{X}$ has a significant dark component and therefore, is not glint. Of course, there is flexibility in this threshold selection. Only those detections that pass the glint test are reported as possibly representing targets.

4. EXPERIMENTAL RESULTS

The first test of the FX algorithm with glint suppression was to verify that glint would not produce significant detection values. The algorithm was applied to six-band multispectral data obtained from the Coastal Systems Station, Dahlgren Division Naval Surface Warfare Center, Panama City Florida. The filter wheel used six different spectral bands to collect the multispectral information. The data contains three background types: a grass field, a beach area without water, and a beach area with water. The first test was on the data containing a beach area with water. Figure 9 shows one of the images used in the first test. Although, the water surface is generally highly reflective, there are some isolated glints that provided a test of the algorithms glint suppression component.

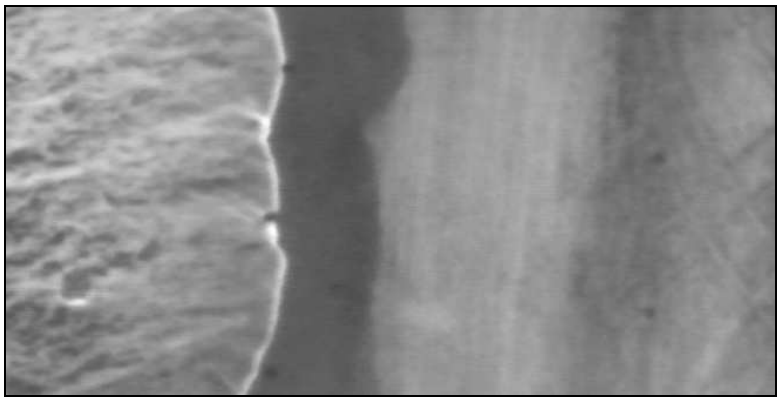

Figure 9: Beach scene with water.

The performance of the base FX algorithm compared to the version with glint suppression for all of the beach and water data is shown in Figure 10. The graph shows the probability of detection versus the probability of false alarm. The glint suppression version clearly demonstrates improved performance.

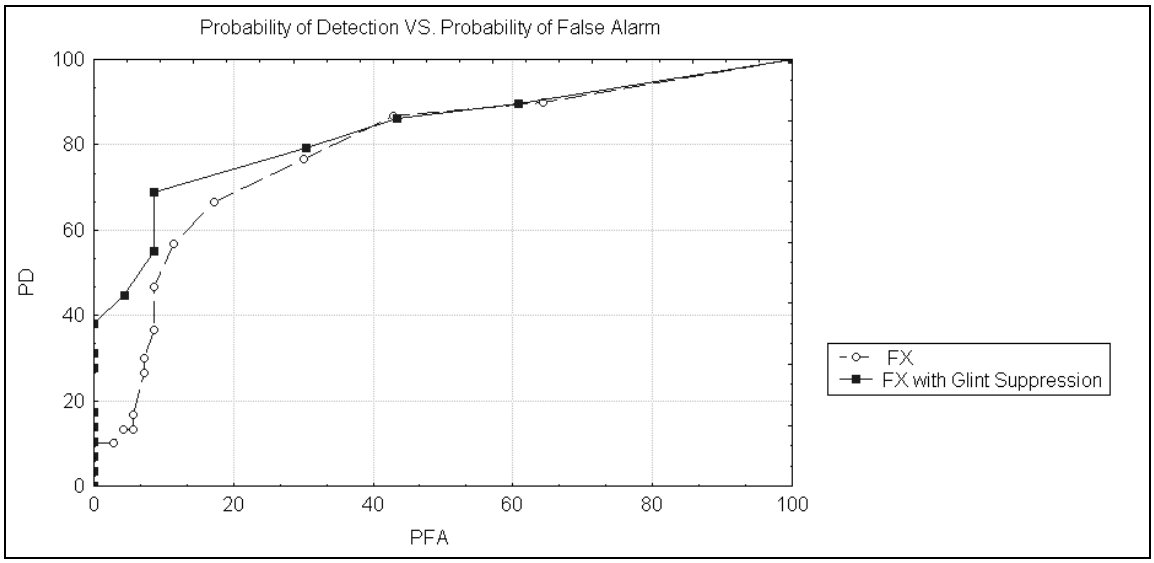

Figure 10: Beach ROC curve.

Next, the algorithm was applied to the beach without water background and the grass background. Examples of these two background types are shown in Figure 12 and Figure 11. Predictably, the baseline algorithm and the glint suppression algorithm produced nearly identical results. The only exception was the elimination of a few false alarms in the grass field by the glint suppression algorithm. However, these were not of sufficient quantity to affect the over all performance.

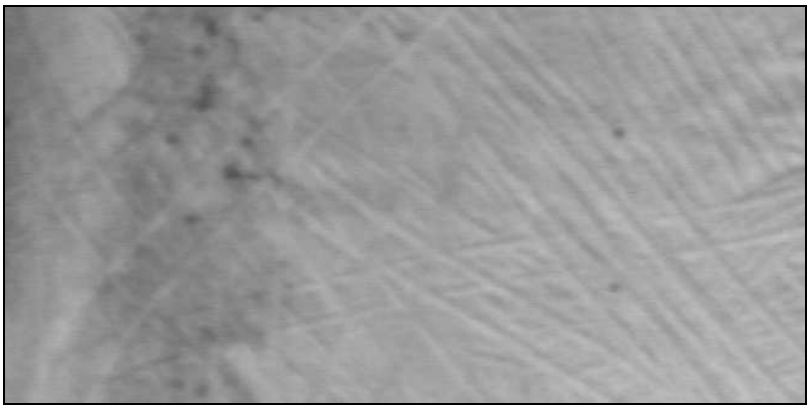

Figure 11: Beach scene without water.

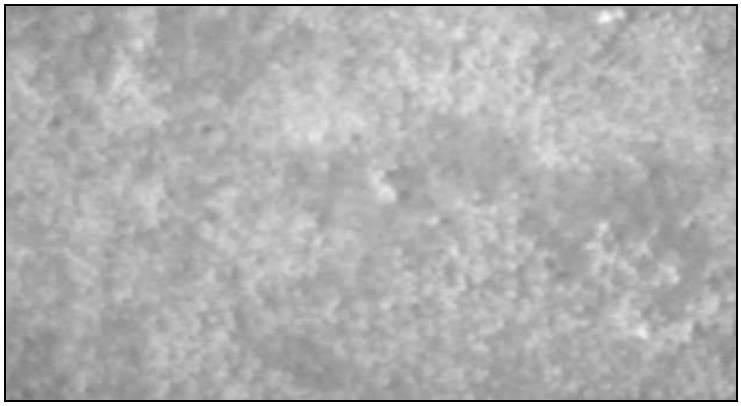

Figure 12: Grass scene.

The final test of the algorithm was on a scene with many isolated glints. Figure 13 show as scene with no true targets and many glints. As expected the algorithm returned zero false alarms for this scene.

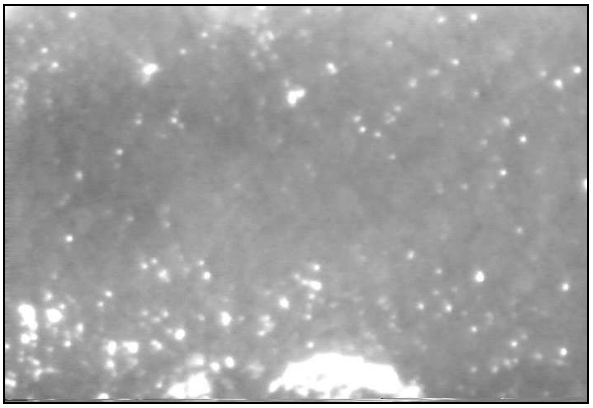

Figure 13: Glint scene.

5. CONCLUSION

The signature adaptive algorithm developed by Crosby and Riley owes much of its success to the limited assumptions placed on the data. However, its adaptability can cause it to be more susceptible to false alarms than matched filter algorithms that depend on a priori target information. The algorithm modification presented in this paper reduces false alarms due to glint while retaining the adaptability of the original target detection method.

Glint often appears as localized anomalies that have the same shape as targets of interest. The similarity in shape prevents discrimination based on morphology. However, the spectral signature of glint is significantly different from most targets. Although the spectral signature of glint is its key feature, it is not invariable and cannot be completely specified.

The calculations of the original detection algorithm can be used to eliminate false alarms due to glint. Choosing a threshold based on the standard deviation selects points with a significant dark component. This negates the effects of glint on detection performance.

ACKNOWLEDGEMENTS

This work was developed under the Office of Naval Research's Advanced Rapid Overt Reconnaissance Algorithms (ARORA) program under execution at the Naval Sea Systems Command, Dahlgren Division, Coastal Systems Station, Panama City Florida.

REFERENCES

[1] Crosby, F. and S. Riley, "Signature Adaptive Mine Detection at a Constant False Alarm Rate", *Proceeding of SPIE Conference on Detection and Remediation Technologies for Mines and Minelike Targets* IV, **4394**, April, 2001.